Monthly Notices
of the
ROYAL ASTRONOMICAL SOCIETY

Mon. Not. R. Astron. Soc. **419,** 164–171 (2012) doi:10.1111/j.1365-2966.2011.19682.x

Signals of exomoons in averaged light curves of exoplanets

A. E. Simon,[1,2⋆] Gy. M. Szabó,[1,2⋆] L. L. Kiss[1,3] and K. Szatmáry[2]

[1]*Konkoly Observatory of the Hungarian Academy of Sciences, PO. Box 67, H-1525 Budapest, Hungary*
[2]*Department of Experimental Physics and Astronomical Observatory, University of Szeged, 6720 Szeged, Hungary*
[3]*Sydney Institute for Astronomy, School of Physics A28, University of Sydney, NSW 2006, Australia*

Accepted 2011 August 23. Received 2011 August 9; in original form 2011 May 25

ABSTRACT

The increasing number of transiting exoplanets sparked a significant interest in discovering their moons. Most of the methods in the literature utilize timing analysis of the raw light curves. Here we propose a new approach for the direct detection of a moon in the transit light curves via the so-called scatter peak. The essence of the method is the evaluation of the local scatter in the folded light curves of many transits. We test the ability of this method with different simulations: Kepler 'short cadence', Kepler 'long cadence', ground-based millimagnitude photometry with 3-min cadence and the expected data quality of the ESA planned planetary transits and oscillations of stars (*PLATO*) mission. The method requires ≈100 transit observations, therefore, applicable for moons of 10–20 d period planets, assuming 3–5 year long observing campaigns with space observatories. The success rate for finding a $1R_{\rm Earth}$ moon around an $1R_{\rm Jupiter}$ exoplanet turned out to be quite promising even for the simulated ground-based observations, while the detection limit of the expected *PLATO* data is around $0.4R_{\rm Earth}$. We give practical suggestions for observations and data reduction to improve the chance of such a detection: (i) transit observations must include out-of-transit phases before and after a transit, spanning at least the same duration as the transit itself, and (ii) any trend filtering must be done in such a way that the preceding and following out-of-transit phases remain unaffected.

Key words: methods: numerical – techniques: photometric – planets and satellites: general – planetary systems.

1 INTRODUCTION

The number of known transiting exoplanets is rapidly increasing, which has recently inspired significant interest as to whether they can host a detectable moon. Although there has been no such example where the presence of a satellite was proven, several methods have already been investigated for such a detection in the future. The most important methods evaluate the timing of transits, e.g., barycentric transit timing variation (TTV; Sartoretti & Schneider 1999; Kipping 2008), photocentric transit timing variation (TTVp; Szabó et al. 2006; Simon, Szatmáry & Szabó 2007), transit duration variation (TDV; Kipping 2009) and time-of-arrival analysis of pulsars (Lewis, Sackett & Mardling 2008). There are further photometric methods for observing rings of exoplanets (Ohta, Taruya & Yasushi 2009; Di Stefano, Howell & Kawaler 2010), starspots in transits (Silva 2003; Silva-Valio et al. 2010, and references therein) or even transits of alien spacecrafts (Arnold 2005).

Here we propose a photometric method for the detection of the moon directly in the raw transit light curves. When the moon is in transit, it puts its own fingerprint on the intensity variation. In realistic cases, this distortion is too little to be detected in the individual light curves. Simply taking the boxcar average of a folded light curve that consists of many transits is not a powerful solution because it results in a significant amount of correlated (pink) noise. The smooth variation of this correlated noise can mimic/hide the real distortions of the light curve due to the moon. Here we introduce the scatter of the folded light curve as an appropriate estimator for the presence of a moon. The stability of the method relies on its robust nature, i.e. the scatter will be estimated in a boxcar that is comparable, or even longer, than the transit duration.

Here we show that a careful analysis of the scatter curve of the folded light curves enhances the chance of detecting the exomoons directly. Our aim is to present a detection technique that is very specific, i.e. when the test is positive, the presence of an exomoon is probable. With careful pre-processing of the light curves (e.g., by recentering the transits), signals that can mimic exomoons are largely suppressed. Consequently, the scatter peak method can be considered both as a tool (i) for quickly finding systems that warrant more detailed analyses and a tool (ii) for confirming the presence of an exomoon when suspected from TTV and/or TDV analyses.

⋆E-mail: atthys@konkoly.hu (AES); szgy@konkoly.hu (GMS)

2 A SIMPLE MODEL FOR THE AVERAGED LIGHT CURVES

2.1 Averaged transit light curves with a moon

Here we describe a very simple model to illustrate the concept of the scatter peak. For the sake of clarity, we consider a special configuration (Fig. 1) that can be handled analytically. Generic transit light curves with a moon will be examined later in numerical simulations.

Let us assume a moon on the circular orbit, and therefore, we a priori know the shape of the light-curve component of the moon (it is similar to that of the planet in shape and duration, but with shallower transit). In this case, the orbital inclination of the moon is 90°. We assume further that the moon orbits slowly, i.e. the moon–planet geometry does not change significantly during the transit, while the transits of the moon appear somewhat earlier or later than the planet's transit. We also make use of the knowledge that TTV was initially removed from data by transforming the time (i.e. shifting the derived transit to the predicted value by recentering, Section 4.1).

Let $f(x)$ be the density function of x, the moon's projected position. Here $x := a_\mathrm{m} * \sin\nu$, where ν is the anomaly and a_m is the semimajor axis of the moon (Fig. 1). Because the orbit is circular, ν follows uniform distribution. After some calculus (see Appendix A for the details) we get the density function of x which is

$$f(x)\mathrm{d}x \propto \frac{1}{\sqrt{a_\mathrm{m}^2 - x^2}}\,\mathrm{d}x. \tag{1}$$

The projected distribution of the moon around the planet follows a $1/\sqrt{a_m^2 - x^2}$ *distribution.*

Because both the transit light curve of the moon, $\mathrm{lc}(t)$ and the averaged light curve is a function of time, $f(x)\,\mathrm{d}x$ must be rewritten to a time domain. If the projected position of the moon is x apart from the planet, the time delay between the transits of the moon and the planet is x/v_orb, where v_orb is the orbital velocity of the planet. The appropriate transformation to the time domain is therefore $\Delta t = x/v_\mathrm{orb}$. Here the relative transit time of the moon $\Delta t = t - t_\mathrm{p}$, where t_p is the time of the transit of the planet. With this notation, the distribution of the transit time of the moon is

$$f(\Delta t)\,\mathrm{d}t \propto \frac{1}{\sqrt{(a_\mathrm{m}/v_\mathrm{orb})^2 - (\Delta t)^2}}\,\mathrm{d}t. \tag{2}$$

In every case, when the moon is observed in an individual light curve, the occulted flux will be the sum of the transit light curve of the planet centred at t_p and the transit light curve of the moon centred at $t_\mathrm{p} + \Delta t$. The light curve of a single event is a convolution of the transit light curve with two Dirac delta functions with different weights, representing the planet and the moon at t_p and $t_\mathrm{p} + \Delta t$, respectively. The average light curve of many events is the expectation flux, taking all ν values into account. At this step, the planet component can be subtracted, and the residual of the moon will remain alone. Since we average many events, the many individual Dirac delta functions representing the moon will follow the distribution of $f(\Delta t)$; thus, the many delta functions in the summation can be simply replaced by a convolution with $f(\Delta t)$. Consequently, the $\mathrm{lc_m}(\Delta t)$ light curve components due to the moon will be averaged to $\overline{\mathrm{lc_m}(\Delta t)}$, which is

$$\overline{\mathrm{lc_m}(\Delta t)} = f(\Delta t) \otimes \mathrm{lc}(\Delta t), \tag{3}$$

where $\otimes$ represents a convolution.

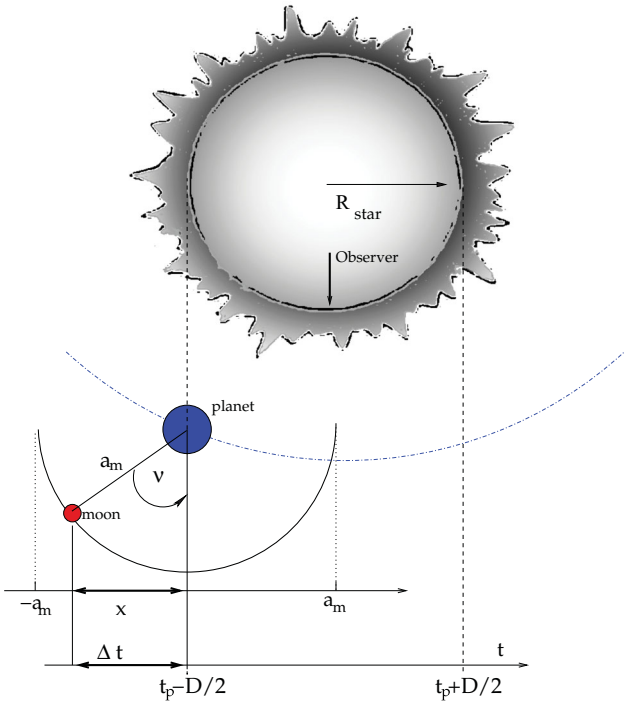

Figure 1. Transit geometry of a star–planet–satellite system.

2.2 The scatter peak

The presence of a moon at a given Δt transit time follows a distribution with a local probability defined in equation (2). Provided that the moon is in fact at the given position, $\mathrm{lc}(\Delta t)$, the light-curve component associated with the moon will be known everywhere. From a set of Δt positions distributed according to equation (2), one can infer the successive distribution of light loss at each generic time τ. In the general case, this distribution will be of the multinomial family, with a non-trivial shape (i.e. if the transit parameters are such that ingress–egress phases are shallower/steeper, there will be more/less probability to detect just little light hidden by the moon). Of course, simulations can easily support parameter-dependent distributions, but for the theoretical framework it is more prudent to consider a very simple light-curve shape: a simple box with the duration (D) and the depth (δm_moon) as free parameters.

Within this framework, the light occulted by the moon at a generic time τ will be equally δm_moon if the moon's position is closer to τ than D ($|\Delta t - \tau| < D/2$) and will be equally zero elsewhere. Hence we know the distribution of the moon itself; this condition on the relative positions can be evaluated; leading to δm_moon, light is occulted by the moon with a probability p expressed by a convolution

$$p(\Delta t) = \int_{\tau - D/2}^{\tau + D/2} f(\Delta t)\,\mathrm{d}\tau \quad \equiv \quad f(\Delta t) \otimes I(|\Delta t - \tau| < D/2) \tag{4}$$

at a generic time τ. Here, $I(C)$ is the identity function which is 1, whereas C is true and 0 elsewhere. With this formulation, the light-curve components due to the moon will be binomially distributed, and the local scatter of light curves can be estimated using the standard deviation of the binomial distribution:

$$\mathrm{rms} = \delta m_\mathrm{m}\sqrt{p(1-p)}, \tag{5}$$

which is the scatter curve of the moon's transit and δm_m is the expected light loss if the single moon is in transit.

Because the precise measurement of scatter requires the analysis of many data points, the light curves will be evaluated in a very

wide long boxcar in practice, to derive precise scatter values. This sampling will behave as a convolution kernel acting on the local values of the scatter, and finally, the shape of scatter curves will be reduced to a simple wide peak (the 'scatter peak') around the transit time of the planet.

In the following section, we examine the scatter peak in real simulations.

3 SIMULATIONS

We made realistic numerical simulations with our image-level simulator (Simon, Szabó & Szatmáry 2009) to examine the discovery probabilities of large exomoons in light curves of different photometric qualities. The reliability analysis (Section 4.1) invokes an accurate estimation of the light-curve scatter and moreover the scatter of the scatter. Because these statistical variables are highly fluctuating, there is a demand for ≈100 transit data for convincing results. Additionally, the same length of data set is required without a moon, interpreting the null signal event. This will be the reference in making the decision whether the detection of the moon is significant. Therefore, all subsets incorporated 109 individual transit light curves. Continuous data sets are delivered by space observatories and even the longest ones from *Kepler* will span about three to five years at most. Hence, the scatter peak is restricted for exomoons around planets with $P_{\rm orb} \lesssim 10$–20 d. That is why we selected $P_{\rm orb} = 10$ d for the model planet. This is also favourable because of the distribution of the currently known exoplanets: the majority of them has orbital periods of this order of magnitude. However, we recall again that the most relevant parameter is not the period of the planet, but the number of transits which we are able to observe.

The planet was a hot Jupiter with $0.7 M_{\rm Jupiter}$, $1.0 R_{\rm Jupiter}$ mass and radius on a circular orbit with $a_{\rm planet} = 0.09$ au. The model moon orbited at $a_{\rm moon} = 6.84 \times 10^5$ km, 82 per cent of the Hill radius and had a period of $P_{\rm moon} = 4.3$ d. This configuration was considered to generally represent a non-resonant case while the moon was enabled to orbit during the transit, and mutual transits were also comprehended. The central star was a solar analogue. Sample light curves of such a system are shown in the top rows of Fig. 2.

Transit light curves of four different qualities were simulated. One data set represented the best quality ground-based (GB) photometry with 178 s sampling and the 0.23 mmag standard deviation of the light-curve points (0.7 mmag error, closely mimicking what has been achieved by Southworth et al. 2010). Space measurements were represented by *Kepler space telescope* short cadence (SC) and long cadence (LC) samplings and the bootstrap noise of non-variable stars. The quality of future space observatories was represented by the anticipated data quality of ESA's planned *PLATO* mission. For the '*PLATO*' quality data set we assumed 25.13 s sampling and an accuracy of 0.12 mmag (data taken from Catala et al. 2011). In such a way, 16 subsets of light curves were calculated, each representing individual systems with different moons (0.5–$1.0 R_{\rm Earth}$ for GB, Kepler LC and SC quality, and 0.4–$1.0 R_{\rm Earth}$ for *PLATO* quality).

4 DETECTION STRATEGY

The secure detection of a moon relies on four important steps. After pre-processing the data, the detection parameters have to be fine tuned, then applied to the observations and finally, we make

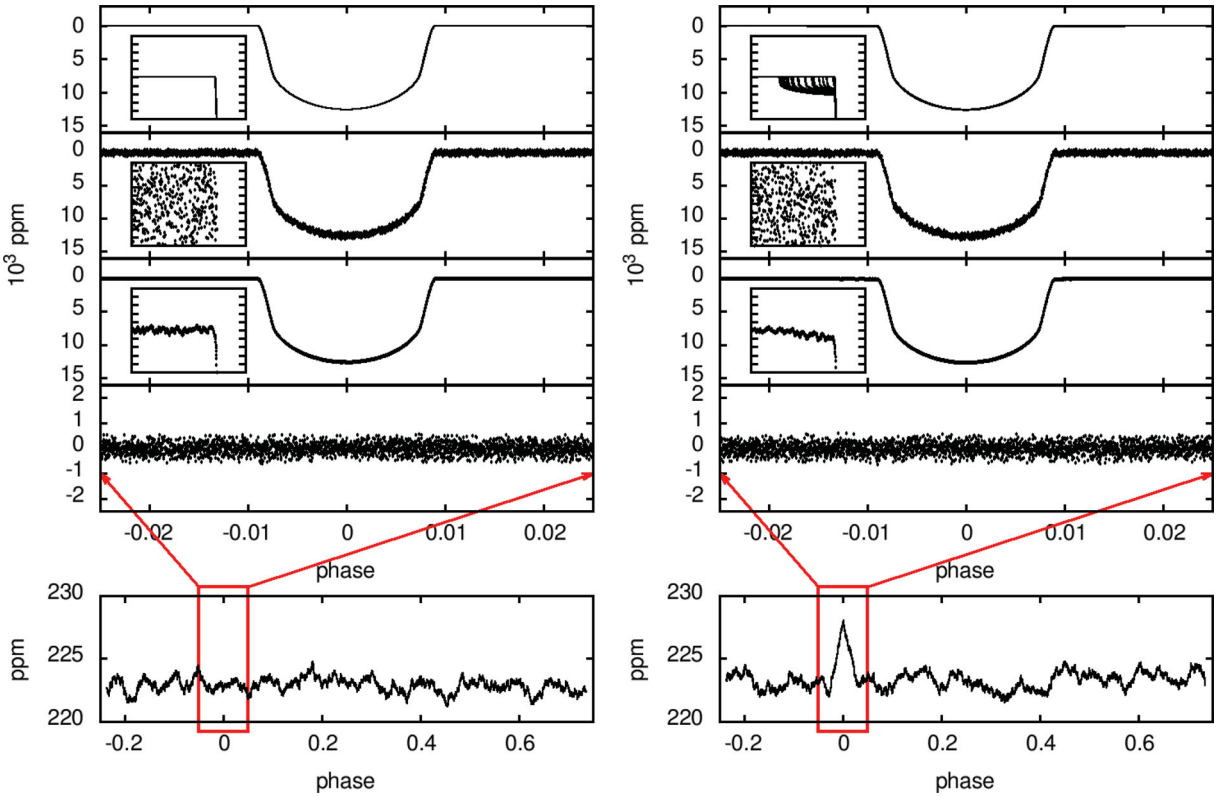

Figure 2. Simulations of 109 transits of a $1 R_{\rm Jupiter}$-sized planet with Kepler SC sampling and noise. Left-hand panel: simulations without a moon; right-hand panel: scatter peak of a $1.0 R_{\rm Earth}$-sized moon. Each column shows the input light curves, the noisified light curves, the median filtered light curves, the residuals to the median and the rms scatter of the residuals (the insets plot the ingress phase of the exomoon; tick step is 50 ppm).

a decision on whether the scatter peak is significant. The detailed recipe of the entire process is as follows.

4.1 Recentering

During pre-processing, the transits must be recentred and stretched to have zero TTV and TDV. This is because there are other sources of TTV and TDV than moons, e.g., perturbing planets. If the folded light curves are still allowed to exhibit such variation of timings and duration, these events will of course result in a scatter peak but not due to the moon. However, if TTV and TDV are removed, and the scatter peak still survives, one will have evidence that there are slight variations in the shape of the transit and its vicinity. Some other processes can lead to similar results, i.e. the stochastic occultation of individual starspots by a single planet. In suspicion of some process leading to systemic light-curve variations, the variations must be modelled specifically before applying the scatter peak evaluation (see also Section 4.4). However, it has to be stressed again that most scenarios with a scatter peak but without a moon can be excluded by recentering; therefore, this step of pre-processing is the most important ingredient of the method.

In this paper, we used simulations with zero TTV and TDV because the mass of the exomoon was forced to be zero in our light-curve simulator. Thus, all detections reflect the photometric effects of the moon itself.

4.2 Boxcar size estimation

The average transit shape is derived from a boxcar median of the folded light curves. The length of the boxcar is a sensitive parameter that must be preset with care. Too little boxcars contain too few points; thus the scatter in the folded light curve and the scatter of the scatter cannot be determined accurately enough. Too large boxcars, on the other hand, cover a longer part of the light curve with significant light variation; therefore, a false scatter peak emerges just because the blurred template differs a lot from the measured light curve. Moreover, the boxcar size will depend on the length and sampling of data, and on the parameters of the planet.

In every case, the boxcar length must be set manually with numerical experiments. A large number of planet transits must be simulated with the same sampling as the data and varying noise. Then, the largest boxcar must be defined which does not produce a false scatter peak with no-moon simulations in the input.

4.3 Evaluation

We experienced optimal boxcar lengths of 249, 25, 749 and 1749 photometric points for the GB, LC, SC and *PLATO* data, respectively. This means that the optimal boxcar was ≈400 s long, regardless of the sampling rate. (This boxcar size corresponds to 1/2200 orbital phase.) Longer boxcars tend to blur the light curve of the planetary transit too much, while shorter boxcars give too noisy results. The use of median is necessary because the signal is little, and the possible outliers have to be eliminated effectively. For such data distributions (e.g. Gaussian noise with distorted wings), the median is a more stable estimate than the mean (Lupton 1995). We have checked the stability of our methods utilizing the mean as the local estimate of light curves, and we indeed experienced that the median is more stable, especially for the length of the boxcar.

In the next step, the median light-curve shape must be subtracted from the observations, leading to the scatter of the light curves (that is, partly due to the signal of the moon if it exists). The scatter peak is there already, but the data distribution is too noisy for an identification. Therefore, smoothing is needed in another boxcar which can be similarly optimized as described above. In our simulations, the second boxcar consisted of 14 999, 1499, 44 777 and 104 999 points (LC, SC, GB and *PLATO* data, respectively), meaning 1.3 times the transit duration. Surprisingly, so long boxcar is necessary to determine the scatter value with appropriate accuracy. When the boxcar is centred at the mid-time of the transit, it can measure the ingress and egress phases of the moon, which may occur well before and well after the transit of the planet, depending on the instant geometrical configuration.

If the exoplanet hosts a moon, a well-defined peak of light-curve scatter appears at the phase of the planetary transits. The height of the peak expresses how significantly the scatter will be increased by systemic light-curve distortions. We normalize the height to the scatter level of the out-of-transit phase. The scatter peak increases with the size of the moon, but its height also depends on the quality of data acquired. In Fig. 3, a set of simulations is shown with the different pre-defined data qualities (in successive columns) and with increasing moon sizes (in successive rows). From this figure, it can be suspected that as large moons as $1 R_{\rm Earth}$ can very likely be detected via the scatter peak.

4.4 Decision making

In the final step, we decide whether there is a convincingly high scatter peak in the data. Even in the no-moon case, the smoothed residuals can mimic a scatter peak just by chance because of numerical fluctuations. A convincingly high scatter peak means such a peak value which infrequently (false alarm probability, FAP) evolves from random fluctuations. A scatter peak is convincing if the specificity, 1-FAP, is close to 1.

The most simple strategy is to observe whether the observed scatter curve exceeds a pre-set threshold level at the time of the transit (i.e. the local scatter is significantly higher than the average scatter plus a few scatters of the scatter, which means that the scatter has really increased, and we do not see the result of simple numerical fluctuations). A lower threshold increases the sensitivity and decreases the size limit, but the FAP worsens if the value is set too low. Balancing between sensitivity and specificity sets up the lowest appropriate threshold level. To do this, we first decide the specificity of the desired detection rate, and then simulate and evaluate many (thousands) of no-moon events. The threshold level belonging to the given specificity is the upper bound of the lowest 1-FAP proportion of scatter peaks. If the observed height of the peak exceeds the threshold level we accept the positive detection.

If one suspects the act of any other process which can lead to a scatter peak, this process must be modelled and incorporated in selecting a threshold level. For example, in the case of an active star, a spotted stellar model can be fitted. The null event has to be simulated with this spotted stellar model, and the threshold level has to be determined in reference to these light curves.

4.5 Weighting

A modified implementation of this method involves the appropriate weighting of photometric residuals, instead of a boxcar smoothing. This will be necessary whenever data of different quality are available. When smoothing in the boxcar (Section 4.4), the expectation for the mean value of the scatter is calculated as, of course,

$$\widetilde{\rm scatter}_{\rm boxcar} = \sqrt{\frac{1}{N}\sum_{\forall i \text{ in boxcar}} r_i^2}, \tag{6}$$

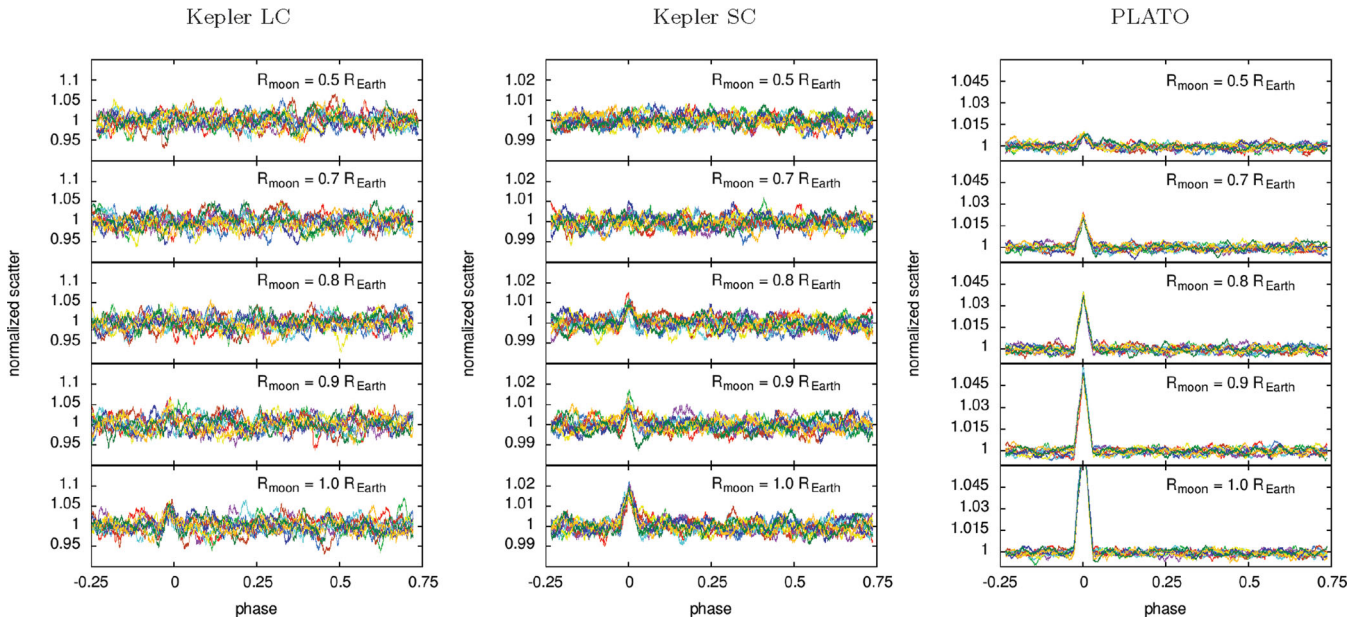

Figure 3. Normalized scatter peaks due to moon transits in sample simulations. Each consecutive row shows 10 curves with Kepler SC, LC and expected *PLATO* simulations. Figure lines show simulations of a $1R_{\rm Jupiter}$ planet with a moon of 0.5, 0.7, 0.8, 0.9 and $1.0R_{\rm Earth}$, respectively.

where r_i is the residuals inside the boxcar, N is the number of data points and $\tilde{}$ denotes an estimate.

If the errors of different data points differ, this formulation requires weighting to keep the least-squares property of our estimator. In this case, the scatter in the boxcar will be estimated as

$$\widetilde{\rm scatter}_{\rm boxcar} = \sqrt{\left(\sum_{\forall i \text{ in boxcar}} \frac{1}{\sigma_i^2}\right)^{-1} \sum_{\forall i \text{ in boxcar}} \frac{r_i^2}{\sigma_i^2}}, \quad (7)$$

where σ_i is the error of the ith data point. Although equation (7) is proportional to the statistic which is usually tested with χ^2 distribution, we keep suggesting a non-parametric evaluation of the weighted scatter, such as described in Section 4.4. This is because χ^2 evaluation assumes that data points come from normal distributions. This is not strictly true in the general case. This improper assumption introduces a little bias, which may easily hide the little signal that we are looking for, or may result in a false alarm. The detection threshold must always be derived from the statistics of the out-of-transit scatter.

5 RESULTS

In Fig. 4, we show simulated detection probabilities and specificity (1-FAP) estimates, expected for GB, Kepler LC, SC and *PLATO*-quality simulated observations. The threshold level is represented in the ordinate, in units of the standard deviation of the scatter curve belonging to the null signal (i.e. out of transit). Decreasing curves (in grey colour) represent the detection probabilities belonging to different size moons, while the black curve plots specificity. We have deduced that for a clear detection (false alarm rate <1 per cent), threshold levels in the 4.3–4.5σ range must be chosen (Fig. 4), almost independently of the quality of the data (sampling rate and scatter).

Somewhat surprisingly, top quality GB observations promise a 30 per cent discovery rate for Earth-sized exomoons, having a scatter peak above the 4.4σ threshold level. Yet we have not got submmag quality observations of $\approx$100 full transits of the same planet, but the increasing number of transit observations and the increasing accuracy of data promise this possibility in the future.

Space telescopes offer a better detection performance only with SC sampling. Selecting 4.4σ threshold, practically all moons of $1R_{\rm Earth}$ size will be discovered in SC (detection rate is 99 per cent.) The 0.9 and 0.8 Earth-sized moons can be discovered with 70 and 20 per cent in Kepler SC data, respectively. The detection limit with *Kepler* is around $0.7R_{\rm Earth}$. These are such large moons which do not exist in the Solar system, but they may be found elsewhere. If such moons exist, they should be discovered in *Kepler* data, and a possible negative result will be a significant implication for the lack of so large moons around hot Jupiters.

Somewhat surprisingly, detection statistics rapidly worsens with longer cadence. We will show that this is primarily a smearing effect (Kipping 2010) rather than a sampling effect. In the top-left panel of Fig. 4, we compared the detection statistics with the Kepler LC curves with instantaneous sampling of the unsmeared light curves ($1R_{\rm Earth}$ size moon, plotted with the dashed line), and the smeared light curve (that is the integrated brightness over the half an hour long exposure, plotted with solid squares and error bars). Selecting a 4.4σ threshold, the detection rate of our model exomoon would be more than 90 per cent with half an hour cadence and without smearing (instantaneous sampling), while it decreases to $\approx$15 per cent if smearing is also included in the model light curves. The detection statistics of smaller exomoons is identical to the distribution of false positives, so in these cases we do not expect success. The striking impairment of the detections is simply due to the severe smearing on the light-curve wings, which blurs the light curve of the planet, suppressing the little-light variations of the moon itself.

A real breakthrough is expected by the *PLATO* mission, which is expected to have significantly lower detection limits (bottom-right panel in Fig. 4). *PLATO* should be able to discover the most exomoons which are larger than $0.6R_{\rm Earth}$ with very low FAP rates. Setting the threshold level to 4.5σ, we expect to discover 40 per cent of the moons with $0.5R_{\rm Earth}$ radius and 7–8 per cent of exomoons with $0.4R_{\rm Earth}$. This experiment will be conclusive in the field of

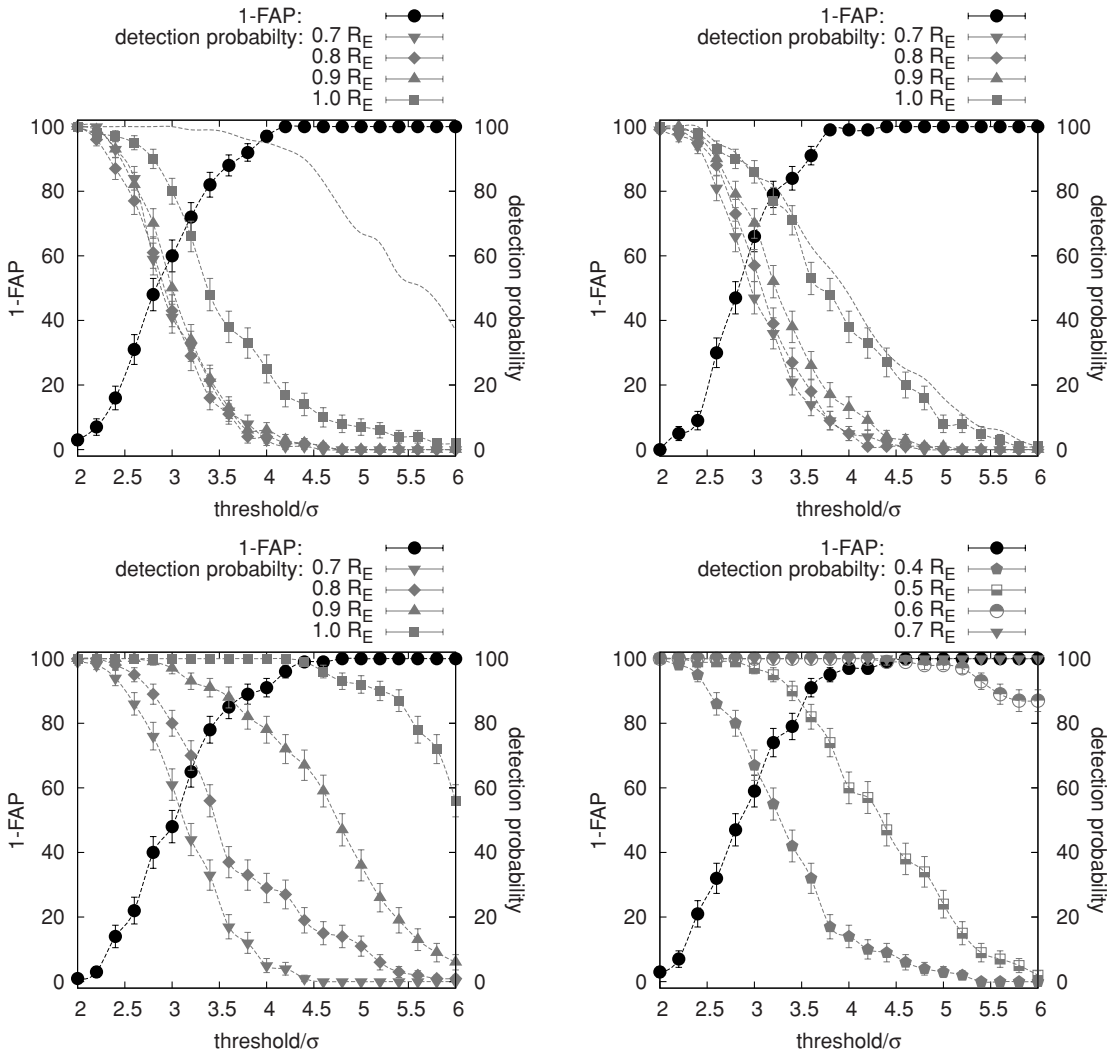

Figure 4. Detection probabilities and specificity levels (1-FAP) at different threshold levels above the background signal with σ standard deviation. Figures show the performance of Kepler LC data (top-left), best quality GB observations (top-right), Kepler SC data (bottom-left) and expected quality of *PLATO* (bottom-right). To illustrate how smearing impairs the detection statistics, in the top panels we plot results from unsmeared reference curves with dashed lines. Smearing does not affect SC sampling (bottom panels). Different-sized moons are colour coded; note that the change in moon sizes in the bottom-right panel.

quest for exomoons: we do know that moons greater than $0.4R_{\rm Earth}$ exist: three moons in our Solar system exceeds this size limit.

5.1 Close-in moons

Besides the size of the moon, the detectability also depends on the orbital radius of the moon. Light-curve effects of close-in moons are limited to the close vicinity of the transit, shortening the time interval when the light-curve distortion is present. This will decrease the scatter of the residuals, and somehow deteriorate the detection statistics. (N.B. close-in moons suffer similar observational limitations with the other methods.) However, the scatter peak method is able to detect at least a part of these kinds of moons. To demonstrate this, we illustrate how the detection statistics worsens for a certain configuration and a single instrument. The complete analysis of close-in moons is a complex multiparametric problem and lies beyond the scope of this paper (see Kipping 2011 for a detailed discussion of a such configuration).

We designed systems consisting of the same planet as in the previous simulations and systematically decreased the orbital radius of the moons to the values of 10, 28, 46, 64 and 82 per cent of the Hill radius. The selected data quality was the *PLATO*-kind sampling and noise, while we observed moons of 0.7, 0.6 and $0.5R_{\rm Earth}$. In Fig. 5, we plot the normalized height of the scatter peak and compare it to the highest peaks by numerical fluctuations in the no-moon case. The heights of the false alarm peaks are plotted with non-continuous lines, while the 4.5σ threshold is denoted by the solid horizontal line. To the left, we plotted the Roche limit, assuming the moon has a density of 3 g cm^{-3}. The symbols show the detection statistics of the 15 probed configurations. Here, one symbol and the interval lines represent a whole distribution of detection success. Therefore, the interval covered by the 'error bar' is the most informative: whenever the error bar goes higher than the threshold level, there are some correct positive detections above 4.5σ level, regardless of the position of the symbol itself.

The plots demonstrate that the detection rate of $0.5R_{\rm Earth}$-sized moons decreases with decreasing the orbital distance; however, the 'error bar' above the solid line expresses that there will be a chance for the detection even at 25–30 per cent of the Hill radius (depending on how lucky configurations occur during the observations). On the

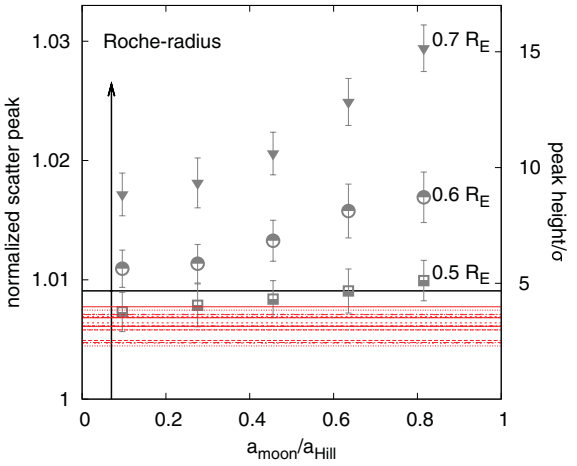

Figure 5. Detection statistics of close-in moons. The peaks occurring by random fluctuations are plotted with various dashed and dotted lines, while the distribution of peak heights in 15 model simulations is plotted by the symbols with error bars. The left axis plots the normalized height of the peak (level of 1 represents the out-of-transit fluctuations), while the right axis plots the height of the peaks above the out-of-transit fluctuations, scaled by σ, the standard deviation of the blurred out-of-transit fluctuations. The threshold level of 4.5 times of the out-of-transit scatter is represented by the solid line.

other hand, the detection success does not decrease for a $0.6 R_{\rm Earth}$ moon (although the significance does decrease, but all systems are detected, since all of them remain above the 4.5σ threshold). The close-in orbits of moons influence the detection statistics only for the moons near the size limit of an observational configuration and does not affect the detection success of larger moons. The observational bias near the low end of moon sizes can be determined with similar numerical experiments, making use of the relevant parameters of the certain system and the quality of the observations as input.

6 DISCUSSION

Besides the scatter peak, several other methods have been proposed which do have the potential of discovering an exomoon (e.g. TTV, TDV, time-of-arrival analysis of pulsars). A significant limitation for such an application is that the transit configuration of the planet can also vary because of perturbations. Hence, the detected variations have to be analysed further and the perturbations must be excluded as the origin of variations. Another limitation is the requirement of having ≈100 transits at least for the analysis, which makes the method to be applicable only for planets with orbital periods of less than 10–20 d. However, this limitation is due to the planned three to five year lifetime of space observatories, and we anticipate that it will be applicable for longer period planets if homogeneous data sets will be available for some transiting systems. Another possible limitation is of physical nature, i.e. more massive moons are more rapidly removed by tidal forces (see Barnes & O'Brien 2002 for a detailed description), while moons beyond ≈0.5 of the Hill radius are not stable on the long time-scale (several billion years in some cases; Domingos, Winter & Yokohama 2006).

In comparison to these methods, scatter peak analysis will be insensitive to perturbation effect in a slightly modified form. If each individual transit is recentred to the estimated position of the planet, the local fluctuations caused by the timing variations will be eliminated. The exact implementation would be 'planetocentric' recentering; for that barycentric TTV is only a good proxy if there is a moon. But in fact any recentering method may be applied here: if there is a moon and we get a positive detection we get what we were looking for. If there is no moon, parametric transit time and the light-curve photocentre (Szabó et al. 2006) coincides exactly, and any of them is appropriate to eliminate planet perturbation effects. The varying position of the moon, however, will still result in systematic variations of the light curve, which will increase the local scatter and, hence, enable to infer that a moon is present. Another advantage is the non-parametric nature of the scatter peak method, which warrants that a priori assumptions of the shape of the transit light curve do not influence the result. We remark that the method is now tested for different moon sizes and orbital radii, while a more general testing (also for inclined and non-circular orbits) is the task of a forthcoming paper. However, the current level of testing does not influence the suggestion that the scatter peak method can help a lot in discovering the exomoons.

ESA's planned *PLATO* mission will offer a great opportunity for the detection of exomoons because of the large number of the targeted stars (≈250 000) and their favourable brightness (8–11 mag). These stars will be mostly cool dwarfs; hence, there will be a good possibility for very accurate radial velocity measurements and to observe the Rossiter–McLaughlin effect in transit. It may be possible to detect the moon in the Rossiter–Mclaughlin effect, too, as a confirmation of the moon, which is independent from the scatter peak (Simon et al. 2010). Kaltenegger (2010) suggested that even the atmosphere of an Earth-sized exomoon can be detected, which is the most important if such an exomoon orbits in the habitable zone (Kipping, Fossey & Campanella 2009).

The most significant error source for the scatter peak method is the quality of de-trending the observed light curves. For space photometry, the slowly changing zero-point of the data could be a significant limiting factor because removing the instrumental trends is everything but trivial. Also, if the detrending of Earth-based photometry involves a comparison of the observation to a set of parametric templates, there will be risk that the algorithm will try to interpret the signal of the moon as systematics and eliminate its signal.

In summary, we conclude that testing the scatter peak from a sequence of light curves is a promising tool for detecting moons directly in the light curves. The success relies on three important conditions as follows.

(i) All light curves must be stacked in such way that the transit time of the planet exactly coincides with each of the analysed light curves.

(ii) Transit observations must include the out-of-transit phases before and after the transit of the planet, where the scatter due to the moon is the highest. The wings must span at least as long as the transit duration.

(iii) Trend filtering of the light curves must be carried out in such a way that small deviations immediately before and after the transit of the planet shall remain unaffected.

ACKNOWLEDGMENTS

This project was supported by the Hungarian OTKA grants K76816 and MB08C 81013, and the 'Lendület' Young Researchers' Program of the Hungarian Academy of Sciences. We thank the referee D. M. Kipping for valuable comments that helped to improve the paper.

REFERENCES

Arnold F. A. L., 2005, ApJ, 627, 534
Barnes J. W., O'Brien D. P., 2002, ApJ, 575, 1087
Catala C., Appourchaux T., PLATO Mission Consortium, 2011, J. Phys. Conf. Ser., 271, 2084
Di Stefano R., Howell S. B., Kawaler S. D., 2010, ApJ, 712, 142
Domingos R. C., Winter O. C., Yokohama T., 2006, MNRAS, 373, 1227
Kaltenegger L., 2010, ApJ, 712, L125
Kipping D. M., 2008, MNRAS, 389, 1383
Kipping D. M., 2009, MNRAS, 396, 1797
Kipping D. M., 2010, MNRAS, 408, 1758
Kipping D. M., 2011, MNRAS, 416, 689
Kipping D. M., Fossey S. J., Campanella G., 2009, MNRAS, 400, 398
Lewis K. M., Sackett P. D., Mardling R. A., 2008, ApJ, 685, L153
Lupton R., 1995, Statistics in Theory and Practice. Princeton Univ. Press, Princeton, NJ
Ohta Y., Taruya A., Yasushi S., 2009, ApJ, 690, 1
Sartoretti P., Schneider J., 1999, A&AS, 134, 553
Silva A. V. R., 2003, ApJ, 585, L147
Silva-Valio A., Lanza A. F., Alonso R., Barge P., 2010, A&A, 510, 25
Simon A. E., Szatmáry K., Szabó Gy. M., 2007, A&A, 470, 727
Simon A. E., Szabó Gy. M., Szatmáry K., 2009, Earth, Moon Planets, 105, 385
Simon A. E., Szabó Gy. M., Szatmáry K., Kiss L. L., 2010, MNRAS, 406, 2038S
Southworth J. et al., 2010, MNRAS, 408, 1680S
Szabó Gy. M., Szatmáry K., Divéki Zs., Simon A., 2006, A&A, 450, 395

APPENDIX A: DERIVING THE PROJECTED POSITION OF THE MOON

We know that ν follows a uniform distribution and the question is the density function of $x = \sin\nu$ (we assume that the length is measured in the unit of a_m for the sake of simplicity). Let $F(\nu) = p(\nu' > \nu)$ and $F(x) = p(x' > x)$ be the cumulative distribution of the same set of positions, parametrized by ν and x, respectively (here p represents probabilities, ν' and x' are generic running parameters). Since ν is uniformly distributed,

$$\frac{\mathrm{d}F(\nu)}{\mathrm{d}\nu} = \frac{1}{\pi} \tag{A1}$$

where ν is the element of the interval $[-\pi/2, \pi/2]$. By the assumption made on the length-scale, $x_\mathrm{m} = \sin\nu$. The differentials of this transformation are $\mathrm{d}x_\mathrm{m} = \cos\nu\,\mathrm{d}\nu$, and because $\cos\nu = \sqrt{1 - x_\mathrm{m}^2}$, $\mathrm{d}\nu = \mathrm{d}x_\mathrm{m}/\sqrt{1 - x_\mathrm{m}^2}$. Substituting $\mathrm{d}\nu$ with $\mathrm{d}x$ leads to the result

$$\frac{\mathrm{d}F(\nu)}{\mathrm{d}x} = \frac{1}{\pi\sqrt{1 - x^2}}, \tag{A2}$$

which is equation (1) of the paper after a_m is written explicitly to represent the appropriate length-scale. Although the expression is singular at the end points ($x/a_\mathrm{m} = \pm 1$), there is no problem with its interpretation because the expression can be integrated everywhere (the question 'What is the probability of having the moon in the outermost 1 per cent of the projected orbit?' can be answered exactly, despite the singularity.)

This paper has been typeset from a TEX/LATEX file prepared by the author.